

# Automated Estimation of the Parameters of Gibbs Priors to be Used in Binary Tomography<sup>1</sup>

Hstau Y. Liao and Gabor T. Herman

*Department of Computer Science  
The Graduate Center  
City University of New York  
New York, USA*

---

## Abstract

Image modeling using Gibbs priors was previously shown, based on experiments, to be effective in image reconstruction problems. This motivated us to evaluate three methods for estimating the priors. Two of them accurately recover the parameters of the priors; however, all of them are useful for binary tomography. This is demonstrated by two sets of experiments: in one the images are from a Gibbs distribution and in the other they are typical cardiac phantom images.

*Key words:* Gibbs distribution, parameter estimation, discrete tomography, Markov random field

---

## 1 Introduction

The reconstruction of a binary image from a few projections (usually only two to four) is a problem of solving a very under-determined system of equations and generally results in a large class of solutions. By using appropriate prior information, the class of possible solutions can be limited to those that are reasonably typical of the class of images, which contains the unknown image that one wishes to reconstruct. *Gibbs priors* describe the local character of an image, which can be viewed as a random sample from a *Gibbs distribution* defined by

$$\pi(f) = \frac{1}{Z} e^{-H(f)}, \quad (1)$$

---

*Email addresses:*

liaoh@hotmail.com (Hstau Y. Liao), gherman@gc.cuny.edu (Gabor T. Herman).

<sup>1</sup> This work was supported by the NIH grant HL70472.

where  $\pi(f)$  is the probability of occurrence of the image  $f$ ,  $Z$  is the normalizing factor, and  $H(f)$  is the *energy* of  $f$ . The rules for calculating  $H(f)$ , for a binary image  $f$ , depend on the values assigned to a finite number (in the examples of our paper this number is two or five) of parameters.

For certain types of Gibbs distributions it has been experimentally demonstrated that there are algorithms that recover an unknown image that is a typical sample from the distribution when provided with the projections of the image and with the values of the parameters of the Gibbs distribution [8]. A difficulty is that in a practical application the parameter values are not known to us. On the other hand, we usually have access to typical images of the application area. The problem that we address is the estimation of the parameters from such sample images for the purpose of reconstruction.

In the rest of this introductory section we make mathematically precise the ideas just introduced, both for Gibbs distribution parameter estimation and for binary tomography. In Section 2 we point out several considerations that can be made in order to reduce the number of parameters that need to be estimated for Gibbs priors. Section 3 gives some examples of images modeled by Gibbs distributions and their reconstructions from three projections. We describe the *Metropolis algorithm*, which is used for generating random samples from a distribution. The Metropolis algorithm can be adapted to find images that approximately satisfy the projections in addition to having relatively high probability of occurrence according to the Gibbs distribution. Section 4 describes three published methods, from [2], [3] and [4], for the estimation of the parameters. In Section 5 we use the squared norm for measuring the success of the estimation process. In Section 6 we evaluate the estimated Gibbs priors from the point of view of their usefulness in binary tomography. Finally, in Section 7 we give some discussions and the conclusions of the paper.

### 1.1 Parameter estimation for Gibbs priors

Let  $D$  be a fixed non-empty finite set that, for reasons that will become immediately obvious, we call the *domain*. In all our examples  $D$  will be a square subset of the square lattice (i.e.,

$$D = \{(i, j) \in \mathbb{Z}^2 \mid 0 \leq i, j < I\}, \quad (2)$$

where  $\mathbb{Z}$  denotes the set of all integers), but the definitions developed here are applicable to an arbitrary  $D$ . A function  $f$  mapping from  $D$  into the set  $\{0, 1\}$  is called a *binary image*. We denote the set of all possible binary images over  $D$  as  $2^D$ . Any non-empty subset of  $D$  is called a *clique*. Given a clique  $q$ , a *configuration* (over  $q$ ) is defined as a function  $g$  mapping from  $q$  into the set  $\{0, 1\}$ . The set of all possible configurations over  $q$  will be denoted as  $2^q$ .

We define a *model* as a pair  $(Q, U)$  in which  $Q$  is a set of cliques and  $U$  is a function mapping the set  $G = \bigcup_{q \in Q} 2^q$  of all possible configurations over all cliques in  $Q$  into the real numbers. We refer to the value  $U(g)$  as the *potential* of the configuration  $g$ . For a model  $\mu = (Q, U)$ , the  $\mu$ -energy of a binary image  $f$  is defined as

$$H_\mu(f) = - \sum_{q \in Q} U(f|q), \quad (3)$$

where  $f|q$  denotes the restriction of  $f$  to the clique  $q$ ; i.e.,  $f|q$  is the configuration  $g$  over  $q$  such that, for all  $d \in q$ ,  $g(d) = f(d)$ . Any model  $\mu$  defines a *Gibbs distribution*  $\pi_\mu$  over  $2^D$  as follows. The probability assigned to a binary image  $f \in 2^D$  is

$$\pi_\mu(f) = \frac{1}{Z} e^{-H_\mu(f)}, \quad (4)$$

where  $Z = \sum_{f' \in 2^D} e^{-H_\mu(f')}$ . (In the discussion below, it will usually be understood what  $\mu$  is at any particular stage. In such a case we will use  $H$  and  $\pi$  instead of  $H_\mu$  and  $\pi_\mu$ , respectively.)

We are now in position to state the general aim of this paper. Suppose that in some application of binary tomography we believe that the efficacy of the process can be improved by modeling the distribution of the binary images as they occur in that application by a Gibbs distribution. Let us assume that the size of the images (and, consequently, of  $D$ ) is fixed. We may also assume (for now) that the set  $Q$  of cliques of the model  $(Q, U)$  is also fixed. (For practical reasons one would try to keep the size of  $Q$  small.) In this case the model (and the resulting Gibbs distribution) is uniquely determined by the values of  $U$ . Typically, there are available to us a number of images which are considered representative samples of images in our application area. Our task is to estimate, based on these sample images, the parameters  $U(g)$ , where  $g \in G$ . (This process may fail in the sense that even with “the best” estimate of these parameters, the model  $(Q, U)$  may not be adequate for modeling the sample images. In this case, we may wish to increase the size of  $Q$ .)

To see the usefulness of image modeling by Gibbs distributions in binary tomography, consider the problem of reconstructing a binary image from its horizontal, vertical, and the NW diagonal projections, under the assumption that the image is a sample from a known Gibbs distribution. If we view the image as a matrix of 0 and 1 entries, then the row (column) sum of the matrix corresponds to the horizontal (vertical) projection of the image. The inputs to the reconstruction problem are: the three projections of the image and the parameters that define the Gibbs distribution from which the image is assumed to be a sample.

At the top-left of Figure 1 is a random sample image from a particular Gibbs distribution. At the top-right is another random sample image from the *same*

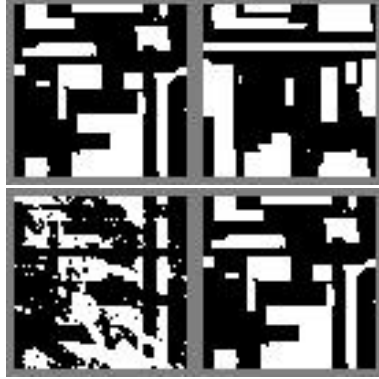


Figure 1. Binary tomography using a Gibbs prior. The top-left image is a random sample from a particular Gibbs distribution. The top-right image is another random sample image from the same distribution. The bottom-left image is a binary image with exactly the same projections (in three directions) as the one at the top-left. By combining both the prior information and the projection data into a reconstruction process, we obtained a perfectly reconstructed image shown at the bottom-right. The number of pixels whose color differs from the color of the corresponding pixel in the top-left image is 1,763 for the top-right image, 822 for the bottom-left image, and 0 for the bottom-right image. The images are all of size  $63 \times 63$ .

distribution. At the bottom-left is a binary image with exactly the same projections (in the three directions) as the one at the top-left. Clearly these three images are very different from each other, which implies that neither one of the two types of information (the projections and the Gibbs parameters) by itself is sufficient for reconstruction. However, by combining the two types of information into a reconstruction process, we obtained a reconstructed image, shown at the bottom-right, which is exactly the same as the the image at the top-left.

This demonstrates the worthwhileness of knowing the parameters that determine the Gibbs distribution from which the unknown image is assumed to be a random sample for the purpose of binary tomography. Further experimental demonstrations of this can be found in [3,8,11].

### 1.2 Binary tomography on $M$ -grids

Following Kong and Herman [7], we define an  $M$ -grid, where  $M$  is an integer greater than 1, as a pair  $(\Gamma, V)$  where

- (1)  $V$  is an ordered set of  $M$  non-zero vectors  $(v_1, \dots, v_M)$  in a Euclidean space (of any dimension), no two of which are parallel, and
- (2)  $\Gamma$  is the set of all linear combinations with integer coefficients of the

vectors in  $V$ ; thus

$$\Gamma = \left\{ \sum_{m=1}^M k_m v_m \mid (k_1, \dots, k_M) \in \mathbb{Z}^M \right\}. \quad (5)$$

From now on, the terms *grid* and *M-grid* ( $M \geq 2$ ) will be used interchangeably. The elements of  $V$  are called the *fundamental direction vectors* of the grid  $(\Gamma, V)$ ; these vectors define the “projection directions” that are used with the grid. If  $d$  is any *grid point* (i.e.,  $d \in \Gamma$ ) and  $v$  any fundamental direction vector of the grid, then the set of grid points  $l = \{d + kv \mid k \in \mathbb{Z}\}$  is called a *grid line*. All examples in this paper will be using the 3-grid  $(\Gamma, V)$  with  $V = \{(1, 0), (0, 1), (-1, 1)\}$  (so that  $\Gamma = \mathbb{Z}^2$ ). Note that the same grid point may correspond to multiple choices of  $(k_1, \dots, k_M)$ ; as in  $-1 \cdot (1, 0) + 1 \cdot (0, 1) + 0 \cdot (-1, 1) = 0 \cdot (1, 0) + 0 \cdot (0, 1) + 1 \cdot (-1, 1)$ .

For a fixed  $M$ -grid  $(\Gamma, V)$ , let the domain  $D$  be a finite non-empty subset of  $\Gamma$ . Given a binary image  $f$ , let  $L^{(m)}$  denote the set of all grid lines that are parallel to  $v_m$  ( $1 \leq m \leq M$ ) and intersect  $D$  (as a consequence, the number of elements in  $L^{(m)}$  is necessarily finite). The *projection* of  $f$  in the direction  $v_m$  is defined to be the function  $P_f^{(m)} : L^{(m)} \rightarrow \mathbb{N}_0$  ( $\mathbb{N}_0$  is the set of non-negative integers) whose values are the *line sums* along the grid lines  $l \in L^{(m)}$ : i.e.,

$$P_f^{(m)}(l) = \sum_{d \in (l \cap D)} f(d). \quad (6)$$

Two binary images  $f$  and  $f'$  are said to be *tomographically equivalent* if  $P_f^{(m)} = P_{f'}^{(m)}$ , for  $1 \leq m \leq M$ .

A *projection data set* on an  $M$ -grid is a collection  $(P^{(1)}, \dots, P^{(M)})$  of functions  $P^{(m)} : L^{(m)} \rightarrow \mathbb{R}$  ( $\mathbb{R}$  denotes the set of real numbers), for  $1 \leq m \leq M$ . Intuitively, the reconstruction problem of binary tomography is to find an  $f$  such that  $P_f^{(m)}$  is “consistent with”  $P^{(m)}$ , for  $1 \leq m \leq M$ . Since such a consistency is the same for all tomographically equivalent images, we can appeal to a Gibbs prior (if one is available to us) to specify the sought-after  $f$  more restrictively. In the following we assume that the Gibbs prior is determined by an energy function  $H$  as in (4). We distinguish between two cases.

*Noiseless case:* We know that  $P^{(m)}$  is exactly  $P_f^{(m)}$  ( $1 \leq m \leq M$ ). In this case it is reasonable to select, from the set of all  $f$  for which  $P_f^{(m)} = P^{(m)}$ , one that minimizes  $H(f)$ , since such an  $f$  has maximal prior probability among all the ones which are tomographically equivalent to it. A method for finding such an  $f$  in the case of a 2-grid is described in detail in [7].

*Noisy case:* In an actual application it is more likely that the  $P^{(m)}$  are only approximations (based on some physical measurements) of the  $P_f^{(m)}$ . In this

case it is reasonable to look for an  $f$  which minimizes

$$H(f) + \alpha \sum_{m=1}^M \sum_{l \in L^{(m)}} |P_f^{(m)}(l) - P^{(m)}(l)|, \quad (7)$$

where the size of the parameter  $\alpha$  indicates our trust in the projection data set as compared to the prior.

For either of these approaches we need an  $H$ , which (provided that the set  $Q$  of cliques is fixed) is uniquely determined by the values of the potentials of all the configurations over all the cliques in  $Q$ . For the rest of this paper we will be concerned with the estimation of these potentials based on sample images.

## 2 Reducing the Number of Parameters

As we stated in the previous section, a Gibbs distribution is uniquely determined by a model  $\mu = (Q, U)$ , where the domain of  $U$  is the set  $G = \cup_{q \in Q} 2^q$  of all possible configurations over  $Q$ . In a very general sense, we can consider a partition  $G = \cup_{c=0}^C G_c$  (where  $G_c \cap G_{c'} = \emptyset$  for  $0 \leq c \neq c' \leq C$ ) of  $G$  such that for all  $g_1$  and  $g_2$  in  $G_c$ ,  $U(g_1) = U(g_2) = U_c$  ( $0 \leq c \leq C$ ). Consequently, the number of parameters to be estimated is reduced to  $C + 1$ . However, it is very easy to show the following property: if a model  $\mu'$  is obtained from a model  $\mu$  by replacing  $U_c$  by  $U_c - U_0$  for  $0 \leq c \leq C$  then, for all images  $f$ ,  $\pi_{\mu'}(f) = \pi_{\mu}(f)$ . Hence we may assume, without loss of generality, that  $U_0 = 0$ , and therefore the number of parameters to be estimated is only  $C$ . (Another assumption, not used in this paper, that one can make based on this property is the non-negativity of the potentials; this is achievable by replacing each  $U_c$  by  $U_c - \min_{c'}(U_{c'})$ .)

The approach of the previous paragraph leads to an interesting simplification of (3) as follows. Given the domain  $D$ , let  $X$  and  $Y$  be two sets of configurations; i.e., if  $x \in X \cup Y$  then  $x : w \rightarrow \{0, 1\}$ , where  $w$  is a nonempty subset of  $D$ . Let  $N(X, Y)$  denote the *number of times an element of  $X$  appears in  $Y$* ; i.e., the number of all possible pairs  $(x, y)$  such that  $x \in X$ ,  $y \in Y$  and  $y$  restricted to the domain of  $x$  is equal to  $x$  (which implies, in particular, that the domain of  $x$  is a subset of the domain of  $y$ ). We note that with this definition  $N(X, Y) = \sum_{x \in X, y \in Y} N(\{x\}, \{y\})$ , where  $N(\{x\}, \{y\})$  is either one (if  $y$  restricted to the domain of  $x$  is equal to  $x$ ) or zero (otherwise). Then it follows that (3) can be re-written as

$$H(f) = - \sum_{c=1}^C N(G_c, \{f\}) U_c. \quad (8)$$

In practice it is desirable to deal with a few parameters rather than with many of them. We now discuss a general approach to producing reasonable partitions of  $G$ . Let  $T$  be a (necessarily finite) set of one-to-one mappings of an element of  $Q$  onto an element of  $Q$  (and so, for every  $t \in T$ , the domain and the range of  $t$  are elements of  $Q$ ). A configuration  $g$  over a clique  $q$  is said to be  $T$ -equivalent to a configuration  $g'$  over a clique  $q'$  if there exists a (possibly empty) sequence  $t_1, \dots, t_S$  of mappings such that

- (1) for  $1 \leq s \leq S$ ,  $t_s \in T$  or  $t_s^{-1} \in T$ ;
- (2)  $q' = \{t_S \cdots t_1(d) \mid d \in q\}$ ; and
- (3) for all  $d \in q$ ,  $g'(t_S \cdots t_1(d)) = g(d)$ .

Clearly,  $T$ -equivalence is an equivalence relation on  $G$ . The partitions that we use to reduce the number of parameters are based on the equivalence classes of such  $T$ -equivalences.

As an example, consider the domain  $D$  of (2) with the set of cliques  $Q$  defined as follows. For  $0 \leq i, j < I$ , define the clique

$$q_{(i,j)} = \{(i \oplus \delta_i, j \oplus \delta_j) \mid \delta_i, \delta_j \in \{-1, 0, 1\}\}, \quad (9)$$

where  $\oplus$  denote addition in  $\mathbb{Z}_I$ ; i.e., addition modulo  $I$ . Let

$$Q = \{q_{(i,j)} \mid 0 \leq i, j < I\}. \quad (10)$$

As examples of one-to-one mappings, consider two mappings of  $q_{(1,1)}$  onto itself: one is a rotation  $\rho$  defined by  $\rho(i', j') = (j', 2 - i')$ , for  $(i', j') \in q_{(1,1)}$ , and the other is a reflection  $\psi$  defined by  $\psi(i', j') = (2 - i', j')$ , for  $(i', j') \in q_{(1,1)}$ . For every  $(i, j) \in D$  we also define two one-to-one mappings  $\tau_{(i,j)}^h$  and  $\tau_{(i,j)}^v$  of  $q_{(i,j)}$  onto  $q_{(i \oplus 1, j)}$  and onto  $q_{(i, j \oplus 1)}$ , respectively, by  $\tau_{(i,j)}^h(i', j') = (i' \oplus 1, j')$ , for all  $(i', j') \in q_{(i,j)}$  and  $\tau_{(i,j)}^v(i', j') = (i', j' \oplus 1)$ , for all  $(i', j') \in q_{(i,j)}$ . The mappings  $\tau_{(i,j)}^h$  and  $\tau_{(i,j)}^v$  are, respectively, a horizontal translation and a vertical translation. If we now let  $T$  contain  $\rho$ ,  $\psi$ , and  $\tau_{(i,j)}^h$  and  $\tau_{(i,j)}^v$  for all  $(i, j) \in D$ , then we find that any configuration defined on a  $3 \times 3$  clique is  $T$ -equivalent to any other configuration which can be obtained from it by translations, rotations around the central pixel, and reflections in either horizontal or vertical central axis. One can reasonably argue that in many applications such  $T$ -equivalent configurations should be assigned the same potential.

We can go further with this idea. Some of these  $3 \times 3$  configurations may be considered to be a particular local feature of one of the following types: a black region, a white region, a convex corner, a concave corner, or an edge. In Figure 2 we give examples of such special configurations. In fact, this set of examples is complete: e.g., a  $3 \times 3$  configuration in an image is a convex corner if, and only if, it is  $T$ -equivalent to one of the configurations identified

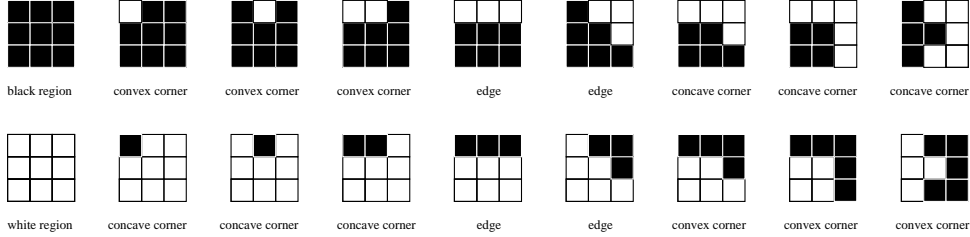


Figure 2. Configurations of a  $3 \times 3$  clique that specify the local features referred to as: a black region, a convex corner, a concave corner, an edge, and a white region.

as a convex corner in Figure 2 (where, for completeness, we may assume that the configurations are over the clique  $q_{(1,1)}$ ). The working definition of these five types of configurations is as follows. A configuration is one of these types only if there are  $k$  consecutive white pixels and  $8 - k$  consecutive black pixels among the eight external pixels of the clique. If the central pixel is black, then the configuration is a black region, a convex corner, an edge, or a concave corner respectively, if, and only if,  $k = 0$ ,  $1 \leq k \leq 2$ ,  $k = 3$ , or  $4 \leq k \leq 5$ , respectively (see the upper row of Figure 2). By switching the color at each grid point of these local features, we will obtain the corresponding “opposite” local features (see the bottom row of the same figure). The opposite of a black region is a white region; the opposite of a convex corner is a concave corner (and vice-versa); the opposite of an edge is still an edge. Here and in the rest of this paper, white (black) pixels will represent grid points with value 1 (0).

A Gibbs distribution based on the five local features of this example can be defined by a model in which  $G = \cup_{c=0}^5 G_c$ , where  $G_0$  is the set of all configurations that are not any of the above specified five local features,  $G_1$  contains the black regions,  $G_2$  the white regions,  $G_3$  the edges,  $G_4$  the convex corners, and  $G_5$  the concave corners. In the rest of the paper we will refer to models of this type as *our models*. The complete specification of one of our models requires the five numbers  $U_1$ ,  $U_2$ ,  $U_3$ ,  $U_4$ , and  $U_5$  (recall that  $U_0 = 0$ ).

We now briefly discuss how a much-studied family of Gibbs distributions can be incorporated into the framework of this section. For an *Ising model*  $(Q, U)$ ,  $D$  is determined by (2) and  $Q$  and the partition of  $G = \cup_{q \in Q} 2^q$  are defined as follows. For  $0 \leq i, j < I$ , let  $q_{(i,j)}^s = \{(i, j)\}$ ,  $q_{(i,j)}^h = \{(i \oplus \delta, j) \mid \delta \in \{0, 1\}\}$  (pair of horizontal neighbors), and  $q_{(i,j)}^v = \{(i, j \oplus \delta) \mid \delta \in \{0, 1\}\}$  (pair of vertical neighbors). The set of cliques  $Q$  is the union of  $Q^s = \{q_{(i,j)}^s \mid 0 \leq i, j < I\}$  and  $Q^p = \{q_{(i,j)}^h \mid 0 \leq i, j < I\} \cup \{q_{(i,j)}^v \mid 0 \leq i, j < I\}$ . The partition  $G = \cup_{c=0}^2 G_c$  is such that a configuration  $g$  is in  $G_1$  if, and only if, it is over some  $q \in Q^s$  and it assigns the value 1 to the single element of  $q$ ; a configuration  $g$  is in  $G_2$  if, and only if, it is over some  $q \in Q^p$  and it assigns the value 1 to both elements of  $q$ ; and the remaining configurations (those that assign to at least one element in their domain the value 0) fall in  $G_0$ . Such an Ising model is completely specified by the pair  $(U_1, U_2)$ . In the Appendix we show

the equivalence of the definition of an Ising model as we have just given it to the more traditional one, such as the one provided by the equation on page 52 of [12]. Here we note that the partition used in our definition could have been obtained by the  $T$ -equivalence classes under a  $T$  consisting of the already defined horizontal and vertical translations, together with a mapping of  $q_{(0,0)}^h$  into  $q_{(0,0)}^v$  by a rotation.

### 3 Image Modeling and Reconstruction

A sample image from a given Gibbs distribution can be generated using a sufficiently long run of the *Metropolis algorithm* [9]. In fact, that algorithm can be used to generate samples from a distribution  $\gamma$  defined on binary images  $f$ , provided that  $\gamma(f) > 0$ , for all  $f \in 2^D$ . The algorithm starts with an arbitrary binary image, and in each step a point  $d$  of the current image  $f$  is randomly selected and its color is inverted, resulting in the image  $\tilde{f}$ . Then  $f$  is replaced by  $\tilde{f}$  with probability  $\min\{1, \gamma(\tilde{f})/\gamma(f)\}$ . To obtain a typical sample from a Gibbs distribution  $\pi$ , we simply set  $\gamma$  to  $\pi$ . For reconstruction, as we will see later, the same approach can be used by defining a distribution which takes into account the prior and the projection data.

#### 3.1 Modeling using Gibbs distributions

In this subsection we show samples from Gibbs distributions defined by some of our models. Specifically, we will consider various choices for the five potentials corresponding to the five types of configurations:  $U_1$  for black regions,  $U_2$  for white regions,  $U_3$  for edges,  $U_4$  for convex corners, and  $U_5$  for concave corners.

We adopt the convention of specifying a particular Gibbs distribution of this type by  $(U_1, U_2, U_3, U_4, U_5)$ . Four random samples of size  $63 \times 63$  from different Gibbs distribution are shown in Figure 3. We can see for example that a higher  $U_3$ , which controls the “edginess”, gives rise to an “edgy” image (bottom-left); while a typical image from a distribution with higher  $U_4$  (for convex corners) has numerous small objects (top-right).

Generation of such sample images using the Metropolis algorithm is computationally feasible because we do not ever have to compute a probability  $\pi(f)$  (which would necessitate the impractically difficult calculation of the factor  $Z$ ) but only the ratio of two different  $\pi(f)$ 's. Another fact which facilitates a low computational burden is that the change of the color of a grid point  $d$  only changes the configuration over cliques which are subsets of the closed neighborhood of  $d$ , a concept which we now define.

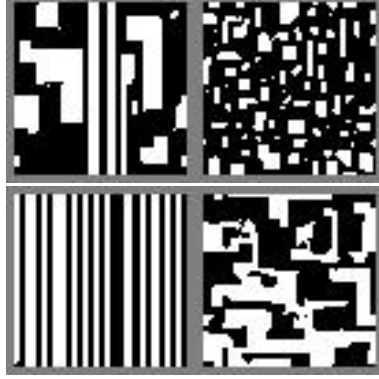


Figure 3. Sample images ( $63 \times 63$ ) from various Gibbs distributions using parameters  $(1.2, 1.2, 1.2, 0.52, 0.2)$  (top-left),  $(1.2, 1.2, 1.2, 0.9, 0.2)$  (top-right),  $(1.2, 1.2, 1.4, 0.52, 0.2)$  (bottom-left), and  $(1.2, 1.2, 1.2, 0.52, 0.6)$  (bottom-right). Note that the difference between the top-left and any other image is caused by a change in only one parameter. With respect to the top-left image the top-right image has a higher  $U_4$  which results in more numerous but smaller objects; the bottom-left image is much more “edgy” since its  $U_3$  is higher; and in the bottom-right image we can see more concavities due to the higher value of  $U_5$ .

Given a set of cliques  $Q$  of the domain  $D$ , the *closed neighborhood*  $\kappa_d$  of  $d \in D$  with respect to  $Q$  is the subset of  $D$  defined by

$$\kappa_d = \{d' \mid \text{for some } q \in Q, d \in q \text{ and } d' \in q\}. \quad (11)$$

and the *neighborhood*  $\sigma_d$  of  $d$  is defined as  $\kappa_d - \{d\}$ . To avoid repetitious discussion of trivial special cases, from now on we assume that a model  $(Q, U)$  is such that, for all  $d \in D$ ,  $\sigma_d$  is nonempty (and so it is a clique, although not necessarily a clique of  $Q$ ). As an example, consider the  $D$  of (2) and let  $Q$  be as defined in (10). Then  $\kappa_{(2,2)}$  comprises  $(2, 2)$  itself and its 24 surrounding points, namely

$$\begin{aligned} &(0, 4) (1, 4) (2, 4) (3, 4) (4, 4) \\ &(0, 3) (1, 3) (2, 3) (3, 3) (4, 3) \\ &(0, 2) (1, 2) (2, 2) (3, 2) (4, 2) \\ &(0, 1) (1, 1) (2, 1) (3, 1) (4, 1) \\ &(0, 0) (1, 0) (2, 0) (3, 0) (4, 0) \end{aligned}$$

Let  $g$  be a configuration over a clique  $q$  and let  $d \in D - q$ . Then we denote by  $g_k^d$  ( $k \in \{0, 1\}$ ) the configuration over  $q \cup \{d\}$  for which  $g_k^d(d) = k$  and  $g_k^d|_q = g$ . We define the *local interaction vector* for  $d$  and  $g$  to be  $a^d(g) = (a_1^d(g), \dots, a_C^d(g))$ , where  $a_c^d(g) = N(G_c, \{g_1^d\}) - N(G_c, \{g_0^d\})$ , for  $1 \leq c \leq C$ .

Using this notation, together with (4) and (8) it is easy to derive that in a

Metropolis step (as described at the beginning of this section)

$$\frac{\pi(\tilde{f})}{\pi(f)} = e^{[1-2f(d)] \sum_{c=1}^C a_c^d(f|\sigma_d)U_c}. \quad (12)$$

For our models, the value of  $\sum_{c=1}^C a_c^d(f|\sigma_d)U_c$  is uniquely determined by the 24-dimensional vector of 0's and 1's provided by the 24 points surrounding  $d$  (in other words, once we know this vector, we no longer need to know what  $d$  is; this is due to the  $T$ -equivalence of configurations under translations). Hence, prior to running the Metropolis algorithm, these  $2^{24}$  possible values can be precalculated and stored in a table. During the running of the algorithm, the needed value is obtained from the table by a simple look-up based on the colors of the points surrounding  $d$  [11].

To insure that the algorithm has been run long enough (*burn in*) to provide a typical sample of the distribution, we made the following experiment. We initialized the Metropolis algorithm with two different images: a blank black image and another which is completely white. Then both cases were run until they stabilized with images of similar energy and similar number of white pixels. The time for the stabilization process is measured in *cycles*: in each cycle,  $63 \times 63 = 3,969$  pixels are randomly selected from the image. In particular, it requires  $2 \cdot 10^4$  cycles for the distributions of Figure 3 to reach stabilization. However, all the samples in the figure were produced by running the algorithm for  $5 \cdot 10^5$  cycles.

### 3.2 Reconstruction using Gibbs priors

Suppose that we wish to reconstruct the top-left image in Figure 1 given its horizontal, vertical, and the NW diagonal projections (i.e., we are considering a 3-grid, whose fundamental directions are  $(1,0)$ ,  $(0,1)$ , and  $(-1, 1)$ ). In the noiseless case, the existence of an image satisfying the projections is assured. However, as is illustrated in Figure 1 at the bottom-left (by an image which is tomographically equivalent to the one at the top-left), the three projections without further information are not sufficient for reconstruction. The principle that we are using to achieve reconstruction is that if we add the information that the image belongs to a particular Gibbs distribution, then the likely solutions will be those which are “close” to the original image [8].

Now consider the noisy case of Subsection 1.2; i.e., the minimization of (7). Define the non-zero valued distribution  $\gamma$  on binary images:

$$\gamma(f) = \frac{1}{Z'} e^{-\beta \left( H(f) + \alpha \sum_{m=1}^M \sum_{l \in L^{(m)}} \left| P_f^{(m)}(l) - P^{(m)}(l) \right| \right)}, \quad (13)$$

where  $\beta > 0$  and  $Z'$  is the normalizing factor. Clearly for a fixed  $\beta$ , the problem of searching for the minimum of (7) is equivalent to the problem of finding the maximum of (13). Note also that the argument which maximizes (13) is the same for any  $\beta > 0$ . In physics, the method of allowing a system of many particles (whose probability distribution resembles (13)) to find a configuration of low energy by slowly increasing  $\beta$  (which corresponds to lowering the temperature) is called *annealing*. Here we use *simulated annealing* by applying the Metropolis algorithm to  $\gamma$  and varying the factor  $\beta$  from a low to a high value. Unlike the standard simulated annealing [5], in our version we keep in the memory the image with the highest  $\gamma$  for a given  $\beta$ , to be used as the initial configuration for the next  $\beta$  in the annealing schedule.

## 4 Parameter estimation

In Figure 1 we have illustrated that if we have the projections of a binary image and the Gibbs distribution from which the image is a sample, then by applying the Metropolis algorithm to (13) with an appropriate annealing schedule, we may obtain a very good reconstruction. Hence, given a typical sample collection of images in a certain application area (we refer to this collection as the *training set* and denote it by  $F$ ), it is worthwhile to estimate a Gibbs distribution which may give rise to such a sample collection. Since a Gibbs distribution is defined by a model  $(Q, U)$ , we need to discover both the set of cliques  $Q$  and the corresponding potentials defined by  $U$ . Here we assume that the set of cliques  $Q$  is given, as well as the partition  $\{G_c \mid 0 \leq c \leq C\}$  of  $G$ , and therefore the only remaining task is to estimate the  $U_c$  for  $1 \leq c \leq C$  (recall that  $U_0 = 0$ ). We discuss a number of previously proposed methods for doing this.

### 4.1 A heuristic approach

This method [3] defines, for  $1 \leq c \leq C$ ,

$$U_c = \kappa[\ln(N(G_c, F)/|G_c| + 1) - \ln(N(G_0, F)/|G_0| + 1)] \quad (14)$$

(recall that  $N(G_c, F)$  is the number of times a configuration in  $G_c$  appears in the training set), where  $|X|$  denotes the number of elements in the set  $X$  and the constant  $\kappa$  is determined by an additional criterion; in this paper we attempt to select  $\kappa$  so that the expected number of white pixels in a sample image from the resulting distribution equals the average number of white pixels in the images of the training set. We note that this constant need not be considered separately in the reconstruction process since it can be absorbed into the  $\beta$  of the annealing schedule.

In the context of Figure 2, a higher potential using this definition implies that the local feature of the corresponding type occurs with a higher frequency in the sample collection.

#### 4.2 The histogram method

This method is based on the previously defined notion of a local interaction vector. The theory behind the method can be found in [4]; see also [10].

Let  $\Omega = \{(d, g) \mid d \in D \text{ and } g \text{ is a configuration over } \sigma_d\}$ . Let us partition  $\Omega$  by the condition that two items belong to the same class of the partition if, and only if, they share the same local interaction vector  $a^d(g)$ . Let  $\Omega = \cup_{b=1}^B \Omega_b$  be this partition and let  $a^b = (a_1^b, \dots, a_C^b)$  be the unique local interaction vector for the elements of  $\Omega_b$ . We also define, for  $k \in \{0, 1\}$  and  $1 \leq b \leq B$ ,  $\Omega_b^k = \{g_k^d \mid (d, g) \in \Omega_b\}$ .

Given the training set  $F$ , the histogram method aims at satisfying, in the least-squares sense, the system of equations

$$\sum_{c=1}^C a_c^b U_c = \ln \frac{N(\Omega_b^1, F)}{N(\Omega_b^0, F)}, \quad (15)$$

for  $1 \leq b \leq B$ . (A hint of the reasonableness of this requirement is provided by (12).) This estimator is well-defined only if  $N(\Omega_b^k, F) \neq 0$  for  $k \in \{0, 1\}$  and  $1 \leq b \leq B$ , which is troublesome since the condition is likely to be violated if we are given a small number of sample images. The elimination of an equation from (15) if either  $N(\Omega_b^0, F) = 0$  or  $N(\Omega_b^1, F) = 0$  can lead to rank-deficiency and preclude a unique solution to the least-squares problem. The advantage of the estimate is that it can be given in closed form and is very easy to calculate. In 1999, Borges [2] proposed two ‘‘improvements’’ to this method which we now discuss.

#### 4.3 Borges’ variant

Theoretical justification of this variant can be found in [2]. The first improvement is the capability to consider cases when either  $N(\Omega_b^1, F) = 0$  or  $N(\Omega_b^0, F) = 0$  by replacing the right hand side of (15) by

$$\Xi(N_1, N_0) = \begin{cases} 0, & \text{if } N_1 = N_0, \\ \frac{1}{N_0+1} + \dots + \frac{1}{N_1}, & \text{if } N_1 > N_0, \\ -\frac{1}{N_1+1} - \dots - \frac{1}{N_0}, & \text{if } N_1 < N_0, \end{cases} \quad (16)$$

where, to simplify notations,  $N_1$  and  $N_0$  denote respectively  $N(\Omega_b^1, F)$  and  $N(\Omega_b^0, F)$ . The second improvement is provided by an estimate of the mean error in the  $\Xi(N_1, N_0)$ . Based on this estimate, we minimize the linear combination of the squared differences, in which the coefficient given to the squared difference arising from the  $b^{\text{th}}$  equation in (15) is  $we_b^2$ , where

$$we_b = \left[ \frac{\pi^2}{3} - \frac{1}{N_0 + N_1 + 1} \sum_{k=0}^{N_0+N_1} \Xi^2(k, N_0 + N_1 - k) \right]^{-\frac{1}{2}}. \quad (17)$$

For  $N_0 + N_1 > 400$ , a good approximation to  $we_b$  is  $\sqrt{3 + 0.05(N_0 + N_1)}$ .

## 5 Evaluation as Modelers

### 5.1 Figure of merit

Suppose that we select a Gibbs distributions using our model, say one of the four illustrated in Figure 3, and we generate some random samples and use them as the training set for a parameter estimation method. The *figure of merit* used in this paper to measure the success of the estimation method is the squared norm:

$$\epsilon = \sum_{c=1}^C (U_c - \tilde{U}_c)^2, \quad (18)$$

where  $U_c$  and  $\tilde{U}_c$  (for  $1 \leq c \leq C$ ) are the actual and estimated values, respectively, of the potentials determining the Gibbs distribution. The recovery (using the histogram and Borges' method) of the parameters of a Gibbs distribution that is slightly more general than what can be obtained by an Ising model was treated in [2]. Although our analysis in this section is, in some sense, more detailed than that of [2], we only report on the results for our model with the five parameters.

### 5.2 Experimental results

In Subsection 3.1, we generated one random sample from each of four Gibbs distributions. Here we take many samples as the input to the estimation processes and report on the behavior of the figure of merit  $\epsilon$  as a function of the number of samples taken.

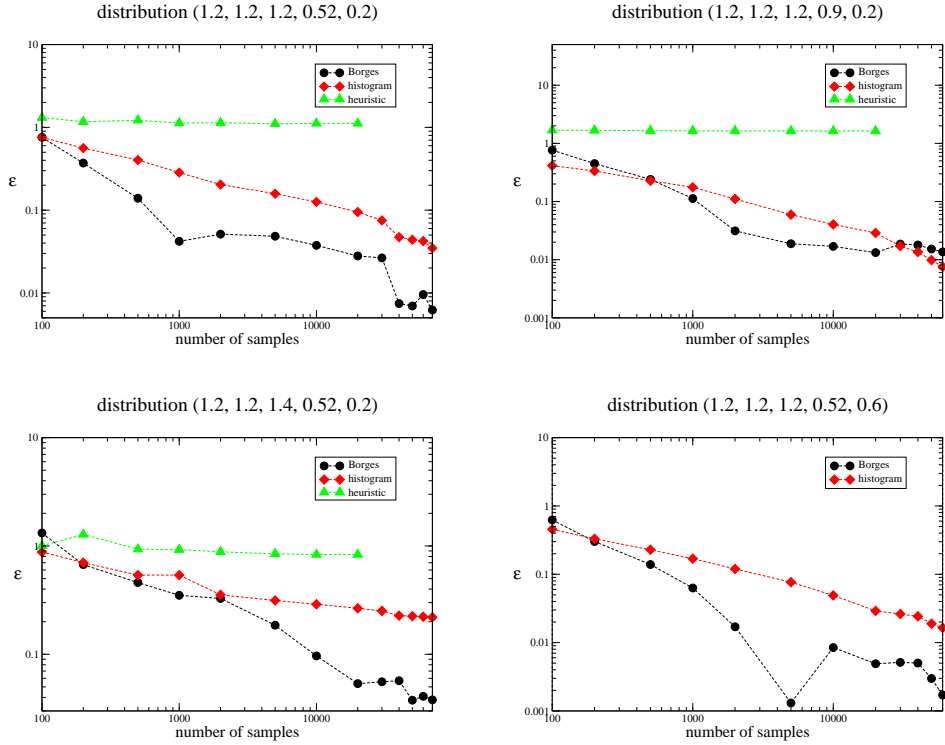


Figure 4. Figure of merit  $\epsilon$  of (18) as a function of the number of samples for the four distributions in Figure 3.

The dependence of  $\epsilon$  on the number of samples for the four distributions is shown in Figure 4. Clearly Borges' method is able to recover the parameters in all the four cases; and so can the histogram method, except that the latter requires, in general, more samples than Borges' method to reach, within a certain tolerance, the original parameters. The heuristic method failed to converge to a similarly low value of  $\epsilon$ . Figure 5 shows typical sample images from distributions estimated by the heuristic method; they do not resemble those from the corresponding original distributions.

We do not report on the heuristic method for the distribution (1.2, 1.2, 1.2, 0.52, 0.6) because its expected number of white pixels is 2,110, while the same item for the distributions defined by (14) applied to the training set is never

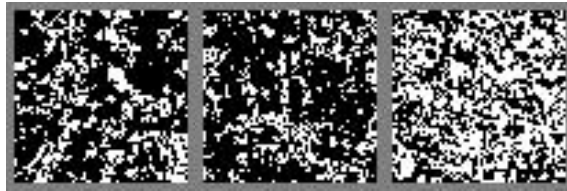


Figure 5. Typical samples from the estimated distribution using heuristic method corresponding to the distribution (1.2, 1.2, 1.2, 0.52, 0.2) (left), (1.2, 1.2, 1.2, 0.9, 0.2) (center) and (1.2, 1.2, 1.4, 0.52, 0.2) (right).

greater than 2,000 for any  $\kappa$ . Thus, our proposed way of selecting the  $\kappa$  in (14) is not guaranteed to produce a result. However, as pointed out already, this is not essential for reconstruction, since the  $\kappa$  can be absorbed into the  $\beta$  of the annealing schedule.

## 6 Evaluation as Priors for Binary Tomography

### 6.1 Introduction: Figure of merit

In this section we discuss our main application of image modeling using Gibbs priors: binary tomography. For a given binary phantom image, we measure the quality of its reconstruction by using the number of points at which the two images differ, and we denote this number by  $\zeta$ . We report on two sets of experiments: in one, called Experiment I, the phantom images are from the Gibbs distribution (1.2, 1.2, 1.2, 0.52, 0.2), in the second one, called Experiment II, we reconstruct cardiac cross-sectional images using estimates of the Ising model ( $\text{II}_1$ ) and of our model ( $\text{II}_2$ ).

### 6.2 Training set, testing set and projection data for Experiment I

The results from the previous section suggest that the estimated parameters can be made to be arbitrarily close (as measured by  $\epsilon$ ) to the original parameters as the size of the training set increases. However, in practice we are not likely to be able to obtain an indefinitely large number of samples; therefore, we restricted the number of samples to be one thousand. As a consequence, the estimated parameters are (1.18, 1.19, 1.19, 0.50, 0.17) by Borges' method and (0.73, 0.49, 0.30, 0.30, 0.19) by the heuristic method. Neither in this experiment nor in Experiment II do we report on the histogram method; this is because, as we have seen in the previous section, its output is indistinguishable from that of Borges' method when the number of samples is large.

For the testing set we generated an additional (to the training set) ten sample images from the same distribution (see Figure 6). For each sample image in the testing set, we took the (noiseless) projections in the three directions (horizontal, vertical, and NW diagonal; i.e., the fundamental direction vectors are, respectively, (1,0), (0,1), and  $(-1, 1)$ ) as the input to the reconstruction process, together with the estimated parameters. All the images are of size  $63 \times 63$ .



Figure 6. Testing set of images that are samples from the distribution (1.2, 1.2, 1.2, 0.52, 0.2).

### 6.3 Training set, testing set and projection data for Experiment II

The phantoms of Experiment II are intended to represent cardiac cross-sectional images and they consist of three geometrical objects of statistically variable size, shape and location: an ellipse representing the left ventricle, a circle representing the left atrium, and the difference between two circular sectors representing the right ventricle. Such a geometrical description defines a function over the subset  $[0, 63) \times [0, 63)$  of  $\mathbb{R}^2$  into  $\{0, 1\}$  and can be digitized by restricting the domain of the function to the  $D$  defined in (2) with  $I = 63$ . Before we can apply the estimation methods of Section 4, we need to decide on the set of cliques  $Q$  and the partition of  $G = \cup_{q \in Q} 2^q$  for this kind of cardiac images. It is far from obvious what those choices should be. In Experiment II<sub>1</sub> we investigate whether the Ising model with two parameters is good enough for the reconstruction of such images, while in Experiment II<sub>2</sub> we use our model with five parameters for the reconstructions.

For the Ising and our model applied to the digitized images described in the last paragraph, Borges' method failed to converge (this is a serious weakness of the method). The reason is the following: if the training images are such that for some  $b$  ( $1 \leq b \leq B$ ) one of the numbers  $N(\Omega_b^0, F)$  and  $N(\Omega_b^1, F)$  is always zero and the other increases with the size of the training set, in order to satisfy (15) (with its right hand side replaced by (16)) for that  $b$ , at least one of the parameters will have to increase without bound. This is the case for the cardiac phantom images, and therefore to avoid the problem we decided to add a little noise to the digitized images. Noise was added by inverting the color of each pixel with probability 0.001 (so that the expected number of pixels whose color is inverted by this process in one of our images of size  $63 \times 63$  is approximately four); the images in Figure 7 were created in this way. To create the images for the training set, the same methodology was used the required number of times; exactly the same training sets were used to estimate the parameters by the heuristic method and by Borges' method. The result-



Figure 7. Digitized noisy cardiac phantom images in the testing set.

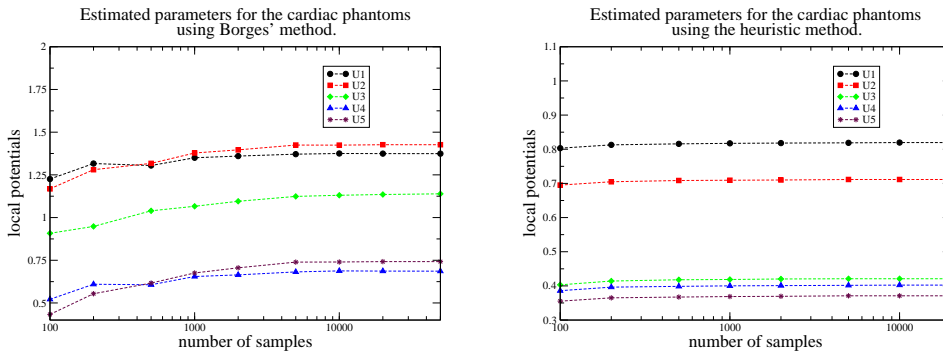


Figure 8. Estimated parameters for our model based on the noisy cardiac phantom images.

ing estimated distributions were  $(0.82, 0.71, 0.42, 0.40, 0.37)$  when using the heuristic method and  $(1.35, 1.38, 1.07, 0.65, 0.68)$  when using Borges' method for our model, and for the Ising model, the methods estimated distributions  $(U_1, U_2)$  equal to  $(-0.36, -0.45)$  and  $(-6.66, 3.46)$ , respectively. In Figure 8 we report on the history of the estimated values of the parameters by the two methods for our model as we increased the size of the training set. Similar curves were obtained for the Ising model. Typical sample images from the estimated distributions based on one thousand training images are shown in Figure 9. Although they do not at all resemble the cardiac phantom images, past experience [3] indicates that they may nevertheless be quite useful for reconstruction.

Physically collected projection data correspond to line integrals through the geometrically defined phantoms. These line integrals may be thought of as “noisy” versions of the line sums, as defined in (6), of the noisy discretized images (of the type shown in Figure 7) that we are trying to reconstruct. The training set is also used to model the nature of the noise in the projection data set. The line sums of the digitized images are always integers, and hence there are only finitely many possible such line sums. Suppose that one of these values is  $p$ ; there will be a number of rows in the noisy cardiac phantom images



Figure 9. Typical samples from the estimated distribution based on our model using the heuristic method (left) and using Borges’ method (the two images at the center). At the right is a typical sample from the estimated distribution based on the Ising model with the parameters estimated by Borges’ method.

in the training set for which the line sums is  $p$ , for each of these rows we can calculate the corresponding line integral through the underlying geometrically defined phantom. Our noise model is predicated on the assumption that the “noisy” version of a horizontal line sum with value  $p$  is a random sample from a Gaussian distribution whose mean and standard deviation are those of the set of line integrals calculated as stated in the previous sentence. Similar calculations are done for horizontal rows with line sums other than  $p$  and, separately, for columns and for diagonals.

Just as in Experiment I, the testing set consists of ten additional binary images, generated by the same method as used to generate those of the training set. Figure 7 shows the images in the testing set. The projection data set for these images were generated using the noise model described in the previous paragraph.

#### 6.4 Experimental details

Once we have the projections data set and the estimated priors, we make the reconstructions by maximizing (13) using the Metropolis algorithm. We then determine the quality of our reconstructions by using the figure of merit  $\zeta$ .

For (13), we need to specify  $\alpha$  (the weighting factor between the prior and the projection data) and the Metropolis algorithm needs an annealing schedule (see Subsection 3.2). To find an optimum  $\alpha$  we start with a gross annealing schedule and find the  $\alpha$  that minimizes the average  $\langle \zeta \rangle$  of the  $\zeta$ ’s over a set of ten training images (independent from the training set used for parameter estimation). The  $\zeta$  for one image is determined in the following way. Each image in this training set is reconstructed five times; the average of the  $\zeta$ ’s over the five reconstructions is what determines the  $\zeta$  for that image. We then refine the annealing schedule and search again for an optimum  $\alpha$  within a neighborhood of the  $\alpha$  previously found. This process is repeated until no significant improvement in  $\langle \zeta \rangle$  is observed.

To specify an annealing schedule, we introduce the following function defined

on  $\lambda$  that denotes the cycle number (see the end of Subsection 3.1) in the Metropolis algorithm:

$$W_{n_1, n_2}^{step}(\lambda) = \begin{cases} 0, & \text{if } \lambda \leq n_1 \cdot step, \\ n_2 - n_1, & \text{if } \lambda > n_2 \cdot step, \\ \left\lceil \frac{\lambda}{step} \right\rceil - n_1, & \text{otherwise,} \end{cases} \quad (19)$$

where for a real number  $r$ ,  $\lceil r \rceil$  denotes the minimum integer greater than or equal to  $r$ .

In Experiment I the optimal  $\alpha$  was estimated to be respectively 1.25 and 3.8 for the priors provided by the heuristic and Borges' method. The corresponding annealing schedules were respectively  $\beta(\lambda) = 96 \cdot W_{0,1}^{5 \cdot 10^4}(\lambda) + 9.6 \cdot W_{1,11}^{5 \cdot 10^4}(\lambda)$  and  $\beta(\lambda) = 30 \cdot W_{0,1}^{5 \cdot 10^4}(\lambda) + 2.5 \cdot W_{1,17}^{5 \cdot 10^4}(\lambda)$ . In Experiment II<sub>1</sub> the optimal  $\alpha$  was estimated to be respectively 60 and 32 for the heuristic method and Borges' method. The corresponding annealing schedules were respectively  $\beta(\lambda) = 4 \cdot W_{0,1}^{3 \cdot 10^4}(\lambda) + 0.5 \cdot W_{1,13}^{3 \cdot 10^4}(\lambda) + W_{13,31}^{3 \cdot 10^4}(\lambda)$  and  $\beta(\lambda) = 10 \cdot W_{0,1}^{3 \cdot 10^4}(\lambda) + W_{1,21}^{3 \cdot 10^4}(\lambda)$ . Finally, in Experiment II<sub>2</sub>, the optimal  $\alpha$  was estimated to be respectively 0.74 and 1.8 for the heuristic method and Borges' method. The corresponding annealing schedules were respectively  $\beta(\lambda) = 134 \cdot W_{0,1}^{5 \cdot 10^4}(\lambda) + 34 \cdot W_{1,9}^{5 \cdot 10^4}(\lambda)$  and  $\beta(\lambda) = 60 \cdot W_{0,1}^{5 \cdot 10^4}(\lambda) + 2.5 \cdot W_{1,4}^{5 \cdot 10^4}(\lambda) + W_{4,16}^{5 \cdot 10^4}(\lambda)$ .

The comparison between the heuristic approach and Borges' method for the two models in the experiments is shown in Table 1. In Figure 10 we show the reconstructed images for phantom number 3 and phantom number 7 using the parameters estimated by both methods for the Ising model and our model.

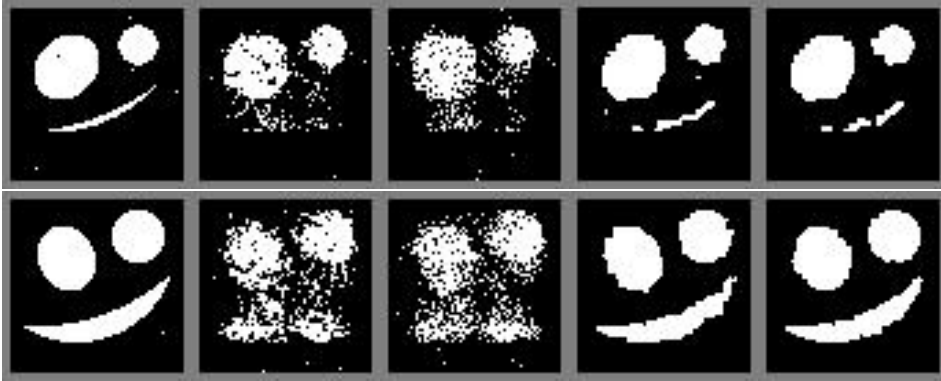


Figure 10. Phantoms number 3 (top) and 7 (bottom) in the first (left most) column along with their respective reconstructed images using Borges' estimated parameters (shown at the second column) and heuristics method's parameters (third column) for the Ising model. Images on the fourth and fifth column are the reconstructions using the two methods' estimated parameters (in the same order) but for our model.

Phantom	Experiment I		Experiment II <sub>1</sub>		Experiment II <sub>2</sub>	
	(1.2,1.2,1.2,0.52,0.2)		Ising model		our model	
	heuristic	Borges	heuristic	Borges	heuristic	Borges
1	1	0	349	297	129	106
2	0	0	335	260	61	91
3	6	0	338	295	168	171
4	6	2	653	643	82	84
5	2	0	216	184	50	128
6	1	4	316	257	84	83
7	1	0	644	624	55	88
8	10	0	304	282	133	121
9	3	0	493	446	67	80
10	2	0	396	343	56	116
$\langle \zeta \rangle$	3	1	405	363	86	107

Table 1

Comparison between the heuristic method and Borges' method for the Ising model and our model in the three experiments. The numbers 1 to 10 in the first column correspond to the images which are the following: in Experiment I these are the samples shown in Figure 6 from the distribution (1.2, 1.2, 1.2, 0.52, 0.2), while in Experiment II they are the cardiac phantom images shown in Figure 7. The rest of entries are values of  $\zeta$  defined as the number of points at which the phantom and its reconstruction (using the indicated priors) differ. The last row reports the average  $\langle \zeta \rangle$  over the ten phantoms rounded to the nearest integer.

## 7 Discussion and Conclusions

In traditional continuous tomography, in which the domain  $D$  is a square shaped subregion of the Euclidean plane and the range of the image  $f$  is the set of real numbers, it is well known (see [6], Section 16.4) that whenever we are given any finite number of views of  $f$  (a view is defined as the integrals of  $f$  along all lines parallel to a given direction), there will be another image that differs from  $f$  in an arbitrarily large manner in a region around any specified point in the domain, which will have the same views as  $f$ . (Note that in spite of this seemingly devastating result, continuous tomography is extremely useful in practice, as is evidenced by the reliance of modern radiology on computed tomography scanners.)

The situation in binary tomography (as presented in this paper) is better: there are well-understood conditions under which the values of a binary image  $f$  are

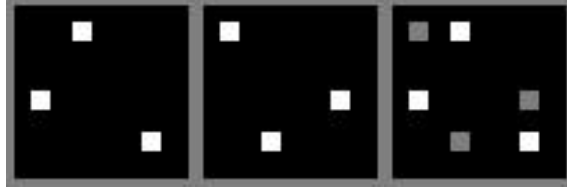


Figure 11. An example in which two very different looking images (left and center) have the same projections in the horizontal, vertical and the NW diagonal directions (see the image at the right to understand why this is so) and also the same energy under one of our models or any Ising model.

uniquely determined from its (noiseless) projections data on an  $M$ -grid (whose definition was given in Subsection 1.2) at certain (well-specified) points of its domain or even over all of its domain [1]. However, such uniqueness cannot always be guaranteed, even if we combine the information in the projection data with the demand that  $H(f)$  be minimized (see Subsection 1.2), as is illustrated in Figure 11. (A little reflection shows that it is reasonable to conjecture that the left and center images in that figure are the only two images that satisfy the projection data for either of them and have minimal energy for our model with  $(1.2, 1.2, 1.2, 0.52, 0.2)$ .)

Examples of non-uniqueness (such as illustrated in Figure 11) have to be carefully designed. Experimental evidence in this and earlier papers [3,8,11] indicates that differences between reconstructed images of the kind illustrated in Figure 11 were hardly ever observed in the situations for which the experiments were carried out, even when the data were noisy. Nevertheless, just as in continuous tomography, there is no absolute guarantee of the accuracy of a reconstruction from projection data on an  $M$ -grid. Users should understand that the generally positive results reported in this and earlier papers are only indicators of the quality that one may *expect* in binary tomography from a few projections, and are not guarantors of similarly good results under all circumstances.

Such positive experimental results motivated us to investigate methods for the estimation of the parameters of Gibbs priors. Section 5 reports on three methods for estimating a Gibbs distribution from sample binary images. Both Borges' method and the histogram method showed successful results for our model with five parameters and converged to the original parameters as the size of the training set increased. This was not the case for the heuristic method. However, in Section 6 it is shown, for one of our models, that the parameters estimated (from samples of the distribution) by all three methods lead to almost perfect reconstructions.

It is also demonstrated in Section 6 that, in spite the fact that our model does not describe adequately the ensemble of the cardiac cross-sectional images, the percent of mis-classified pixels in a typical reconstruction is below

three (as opposed to ten in the Ising model), which may well be sufficiently small to provide useful information regarding the cardiac structures which are being imaged. The fact that the reconstructions with our model are better qualitatively and quantitatively than with the Ising model shows that for this application of cardiac imaging the larger cliques are more suitable. The smaller cliques in the Ising model result in much less adequate reconstructions.

## Appendix

For an Ising model as defined in [12] (page 52), the energy (expressed using the notations and conventions of this paper) is defined by

$$\begin{aligned}
H(f) = & -U_1^{Ising} \sum_{\{(i,j)\} \in Q^s} [2f(i,j) - 1] \\
& - U_2^{Ising} \sum_{\{(i,j),(i',j')\} \in Q^p} [2f(i,j) - 1][2f(i',j') - 1],
\end{aligned} \tag{20}$$

where  $U_1^{Ising} = \frac{J}{kT}$  and  $U_2^{Ising} = \frac{mB}{kT}$ . (For the discussions that follow, the precise meanings of the physical constants  $J$ ,  $k$ ,  $T$ ,  $m$ , and  $B$  are irrelevant.)

Noting that

$$\sum_{\{(i,j),(i',j')\} \in Q^p} f(i,j) = \sum_{\{(i,j),(i',j')\} \in Q^p} f(i',j') = 2 \sum_{\{(i,j)\} \in Q^s} f(i,j) \tag{21}$$

and observing (a trivial consequence of (4)) that if the difference between two energies  $H(f)$  and  $H'(f)$  is a constant, then the corresponding Gibbs distributions are the same, we get that the Gibbs distribution whose energy is  $H(f)$  is identical to the Gibbs distribution whose energy is

$$\begin{aligned}
H'(f) = & -(2U_1^{Ising} - 8U_2^{Ising}) \sum_{\{(i,j)\} \in Q^s} f(i,j) \\
& - 4U_2^{Ising} \sum_{\{(i,j),(i',j')\} \in Q^p} f(i,j)f(i',j').
\end{aligned} \tag{22}$$

Using the notion introduced in Section 2, we see that the term  $\sum_{\{(i,j)\} \in Q^s} f(i,j)$  in (22) is  $N(G_1, \{f\})$  and the term  $\sum_{\{(i,j),(i',j')\} \in Q^p} f(i,j)f(i',j')$  in (22) is  $N(G_2, \{f\})$ . Hence, by (8), our definition of an Ising model will give rise to the same Gibbs distribution as defined by (20), provided only that  $U_1 = 2U_1^{Ising} - 8U_2^{Ising}$  and  $U_2 = 4U_2^{Ising}$ . Clearly, the converse is also the case: any Gibbs distribution defined using our definition of an Ising model can also be obtained by the appropriate selection of  $U_1^{Ising}$  and  $U_2^{Ising}$  in (20).

## References

- [1] R. Aharoni, G.T. Herman, and A. Kuba, Binary vectors partially determined by linear equation systems, *Discrete Mathematics* **171** (1997), 1–16.
- [2] C.F. Borges, On the estimation of Markov random field parameters, *IEEE Trans. Pattern Anal. Mach. Intell.* **21** (1999), 216–224.
- [3] B.M. Carvalho, G.T. Herman, S. Matej, C. Salzberg, and E. Vardi, Binary tomography for triplane cardiography, in: A. Kuba, M. Samal and A. Todd-Pokropek, eds., *Information Processing in Medical Imaging* (Springer, Berlin, 1999) 29–41.
- [4] H. Derin and H. Elliot, Modeling and segmentation of noisy and textured images using Gibbs random fields, *IEEE Trans. Pattern Anal. Mach. Intell.* **9** (1987), 39–55.
- [5] R.O. Duda, P.E. Hart, and D.G. Stork, *Pattern Classification* (John Wiley & Sons, New York, 2001).
- [6] G.T. Herman, *Image Reconstruction from Projections: The Fundamentals of Computerized Tomography* (Academic, New York, 1980).
- [7] T.Y. Kong and G.T. Herman, Tomographic equivalence and switching operations, in: G.T. Herman and A. Kuba, eds., *Discrete Tomography: Foundations, Algorithms and Applications* (Birkhäuser, Boston, 1999) 59–84.
- [8] S. Matej, G.T. Herman and A. Vardi, Binary tomography on the hexagonal grid using Gibbs priors, *Int. J. Imag. Sys. and Tech.* **9** (1998), 126–131.
- [9] N. Metropolis, A.W. Rosenbluth, M.N. Rosenbluth, A.H. Teller, and E. Teller, Equations of state calculations by fast computing machines, *J. Chem. Phys.* **21** (1953), 1087–1092.
- [10] S.G. Nadabar and A.K. Jain, Parameter estimation in Markov random field contextual models using geometric models of objects, *IEEE Trans. Pattern Anal. Mach. Intell.* **18** (1996), 326–329.
- [11] E. Vardi, G.T. Herman, T.Y. Kong. Speeding up stochastic reconstructions of binary images from limited projection directions. *Linear Algebra and its Applications*, **339** (2001), 75–89.
- [12] G. Winkler, *Image Analysis, Random Fields and Dynamic Monte Carlo Methods* (Springer, Berlin, 1995).